



## Direct *ab-initio* molecular dynamic study of ultrafast phase change in Ag-alloyed $\text{Ge}_2\text{Sb}_2\text{Te}_5$

B. Prasai, G. Chen, and D. A. Drabold<sup>a)</sup>

Department of Physics and Astronomy, Ohio University, Athens, Ohio 45701, USA

(Received 13 November 2012; accepted 16 January 2013; published online 29 January 2013)

We employed *ab-initio* molecular dynamics to directly simulate the effects of Ag alloying (less than 5% Ag concentration) on the phase change properties of  $\text{Ge}_2\text{Sb}_2\text{Te}_5$ . The short range order is preserved, whereas a slight improvement in the chemical order is observed. A slight decrease in the fraction of tetrahedral Ge ( $\text{sp}^3$  bonding) is reflected in the reduction of the optical band gap and in the increased dielectric constant. Simulations of the amorphous to crystalline phase change cycle revealed the fact that the crystallization speed in  $\text{Ag}_{0.5}\text{Ge}_2\text{Sb}_2\text{Te}_5$  is not less than that in  $\text{Ge}_2\text{Sb}_2\text{Te}_5$ . Moreover, the smaller density difference and the larger energy difference between the two phases of  $\text{Ag}_{0.5}\text{Ge}_2\text{Sb}_2\text{Te}_5$  (compared to  $\text{Ge}_2\text{Sb}_2\text{Te}_5$ ) suggest a smaller residual stress in devices due to phase transition and improved thermal stability for  $\text{Ag}_{0.5}\text{Ge}_2\text{Sb}_2\text{Te}_5$ . The potential viability of this material suggests the need for a wide exploration of alternative phase change memory materials. © 2013 American Institute of Physics. [<http://dx.doi.org/10.1063/1.4789877>]

The computational design of materials is still in its nascent stages but is widely recognized to be one of the prime frontiers of materials science. The challenges are daunting for several reasons, among these: time and length scales drastically differ in simulation compared to laboratory samples; the need for realistic interatomic interactions (nowadays largely based upon pseudopotentials and density functional theory) leads to tremendous demand for computational resources. In the case of the phase change memory materials, with compositions near  $\text{Ge}_2\text{Sb}_2\text{Te}_5$  (GST), there is clear evidence that current first principles simulations can accurately simulate phase changes on the time scales accessible to these codes.<sup>1</sup> Other work suggests that key quantities like crystallization speed can be meaningfully inferred from such simulations.<sup>1</sup> These materials are of fundamental interest for their ultrafast phase changes and are the leading candidate to replace current non-volatile computer memory, a multi-billion dollar market.

In this paper, we explore candidate phase change materials and show that a silver-doped variant may be superior to conventional GST. We elucidate the process of crystallization in atomistic detail and particularly note the role of the Ag in producing more stable and chemically ordered materials. Because this initial study with Ag suggests the need for further research, it is likely that other materials will also be found in a similar way, warranting additional investigation.

We have implemented an *ab-initio* molecular dynamic (AIMD) simulations to study the ultrafast crystallization of Ag-doped (alloyed) $\text{Ge}_2\text{Sb}_2\text{Te}_5$ . The AIMD calculations were performed using Vienna *Ab-initio* Simulation Package (VASP)<sup>2-4</sup> to generate models of  $\text{Ge}_2\text{Sb}_2\text{Te}_5$  and  $\text{Ag}_{0.5}\text{Ge}_2\text{Sb}_2\text{Te}_5$  (AGST) with 108 (24 Ge atoms, 24 Sb atoms, and 60 Te atoms) and 114 (24 Ge atoms, 24 Sb atoms, 60 Te atoms, and 6 Ag atoms) atoms, respectively. The calculations were performed by using the projector augmented-wave (PAW)<sup>5,6</sup> method to describe electron-ion interactions. The Perdew-Burke-Ernzerhof (PBE)<sup>7</sup>

exchange correlation functional was used throughout. Molecular-dynamics (MD) simulations were performed in a cubic supercell with a time step of 5.0 fs using periodic boundary conditions at constant volume for annealing, equilibrating, and cooling, whereas zero pressure conjugate gradient (CG) simulations were performed for relaxation. The final models were prepared by using the “Melt and Quench” method<sup>8</sup> starting with a random configuration at 3000 K. Densities of  $6.046 \text{ g cm}^{-3}$  and  $6.234 \text{ g cm}^{-3}$ , respectively, for GST and Ag-GST, were used during the process. After mixing the random configurations at 3000 K for 20 ps, each model was cooled to 1200 K in 10 ps and equilibrated for 60 ps. A cooling rate of 12 K/ps was adopted to obtain the amorphous models from the melt at 1200 K to 300 K and followed by equilibration at 300 K for another 50 ps. Finally, the systems were fully relaxed to a local minimum at zero pressure. Three different models were generated for each of the structures. For the illustration purpose, one such zero-pressure structure, each of amorphous GST and AGST, is presented in Figs. 1(a) and 1(b).

To investigate the ultrafast crystallization, we annealed the a-GST and a-AGST models at 650 K until each of the models crystallized. Figs. 1(c) and 1(d) show fully relaxed structures of c-GST and c-AGST, respectively. The full potential of simulation is revealed in directly simulating phase transitions.<sup>1,9,10</sup> The whole crystallization process proceeds in three steps (I, II, and III), as explained by Lee and Elliott.<sup>10</sup> Period I is termed the incubation period. Period II is the main time segment in which the process of crystallization occurs, and the third period (III) defines the completely crystallized state. To understand the crystallization process, we observed the evolution of total energy of the system, the number of 4-member rings, seeds in the spirit of classical nucleation theory (CNT),<sup>10</sup> the number of wrong bonds (bond pairs other than Ge-Te, Sb-Te, and Ag-Te are termed as “wrong bonds”<sup>1</sup>), and the total coordination numbers as a function of time and presented in Figs. 2(a)–2(d). We observe almost no change in the total energy and the number of 4-member rings during the incubation period (I); however,

<sup>a)</sup>Electronic mail: drabold@ohio.edu.

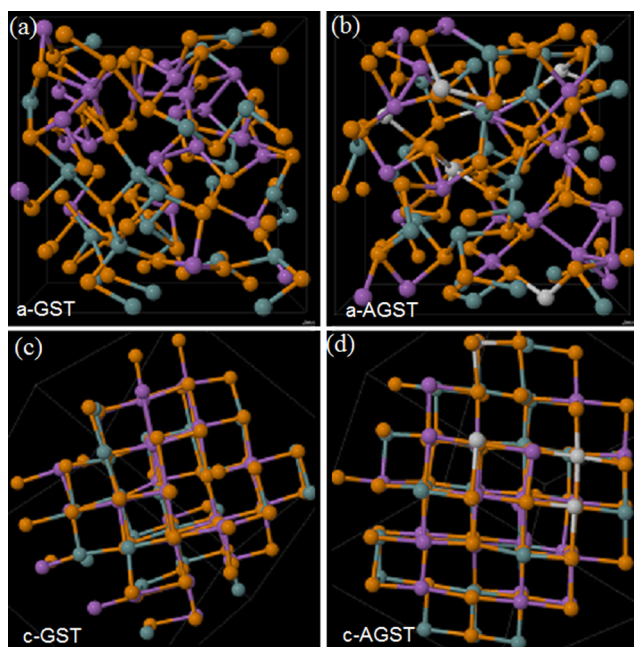


FIG. 1. Relaxed models of (a)  $a\text{-Ge}_2\text{Sb}_2\text{Te}_5$ , (b)  $a\text{-Ag}_{0.5}\text{Ge}_2\text{Sb}_2\text{Te}_5$ , (c)  $c\text{-Ge}_2\text{Sb}_2\text{Te}_5$ , and (d)  $c\text{-Ag}_{0.5}\text{Ge}_2\text{Sb}_2\text{Te}_5$  (model 3). Color code: orange-Te, green-Ge, purple-Sb, and gray-Ag.

we observe a significant decrease in the number of wrong bonds. Wrong bonds keep declining during the crystallization period (II) until the crystallization is complete. After crystallization,  $\sim 5\%$  homopolar bonds persist. The total energy and the number of 4-member rings are found to be correlated to each other, with the number of rings increasing monotonously during the crystallization period. We further computed the evolution of pair correlation functions and the Ge-centered bond angle distribution (for model 3) and present these findings in Figures 3 and 4, respectively. The top panels of Fig. 3 represent the total pair correlation functions (TPCF). The middle panel on the left represents the X-Te (where X=Ge and Sb) pair correlation functions, whereas

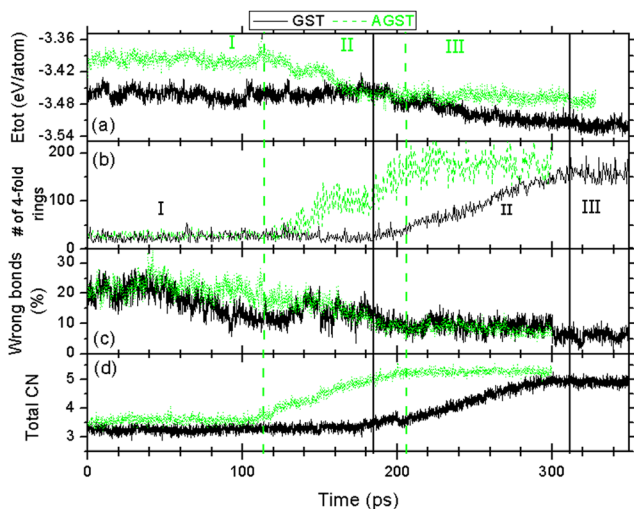


FIG. 2. Comparison of the total energy (a), the number of four-fold rings (b), the number of wrong bonds (c), and the total coordination numbers (d) as functions of time in  $\text{Ge}_2\text{Sb}_2\text{Te}_5$  (dark, black) and  $\text{Ag}_{0.5}\text{Ge}_2\text{Sb}_2\text{Te}_5$  (light, green) (model 3). The vertical lines separate the three periods.

that on the right represents X-Te (X=Ge, Sb, and Ag) PCFs. Finally, the bottom panels represent the correlation of wrong bonds (Y-Y, Y=Ge, Sb, or Ag, and Te-Te). These figures depict the evolution of medium to long range order (secondary peaks in PCFs), the signature of crystalline order. The prominent medium to long range order peaks start evolving during period II. The average peak positions at 2.98 Å, 5.3 Å, and 6.8 Å for X-Te, and 4.2 Å and 7.4 Å for wrong bonds well represent the crystalline GST structure. Similarly, the Ge-centered bond angle distribution (BAD) (Fig. 4) shows an evolution of narrow and prominent distribution around  $90^\circ$  and  $180^\circ$  during period II. The narrowing of the peak at  $90^\circ$  illustrates the conversion of the tetrahedral Ge (angular distribution at  $109^\circ$ ) into the octahedral Ge. The peak at around  $180^\circ$  becomes visible during period II where the total coordination numbers (CN) reach about 4.5, similar to the evolution of secondary peaks in partial pair correlation functions (PPCFs). CN on the other hand depicts a correlation with the total energy of the system, i.e., CN is almost constant during the incubation period (I), increases during the crystallization period (II), and becomes constant after the crystallization is established.

Since the crystallization of three different models of pure GST shows large fluctuations in the duration of periods I and II, especially period I, the estimation of crystallization time involves significant uncertainty. The incubation periods (period I) in three different pure GST models vary from 50 ps to 200 ps, whereas the crystallization periods (Period II) vary from 40 ps to 150 ps. These times in AGST are (80–110 ps) for incubation periods and (70–110 ps) for crystallization periods. To understand this large deviation in the incubation as well as the crystallization periods, we examined the structure of the starting configuration of the three GST models. We observe various numbers of wrong bonds and four membered rings, and the model with the short incubation and crystallization period has the least number of wrong bond and the most number of four membered rings (more ordered in a plane). To compare crystallization speeds, we inspected the models of GST and AGST with similar initial fractions of wrong bonds. We observed a clear contrast in the duration of both the incubation period and the crystallization period in these two networks. Both of the periods were shorter in AGST than in GST. Total of these two periods in AGST measure about 200 ps against about 315 ps in pure GST, hinting at a faster crystallization in Ag-doped GST.

Now, to understand the faster crystallization of AGST as compared to GST, we examined local structures of the models. Each of these models (both amorphous and crystalline phases) was equilibrated at 300 K for 25 ps. To investigate the Ag-induced modification of GST network, we analyzed the local structure via PPCFs and BADs. Except for wrong bonds, the PPCFs and BADs show no dependence on the models and hence only model 3 PPCFs and BADs are presented for the illustration purpose. We inspected the Ge-Te PPCF (Fig. 5) and Ge-centered BAD (Fig. 6) because Ge atoms undergo a dramatic change upon phase transition, i.e., perfect octahedral configurations (p-bonding) in the crystalline phase and tetrahedral geometry ( $\text{sp}^3$ -bonding) in the amorphous phase.<sup>11</sup> In the amorphous phase, the Ge-Te bond length is found to be increased (by 0.02 Å) in Ag-doped

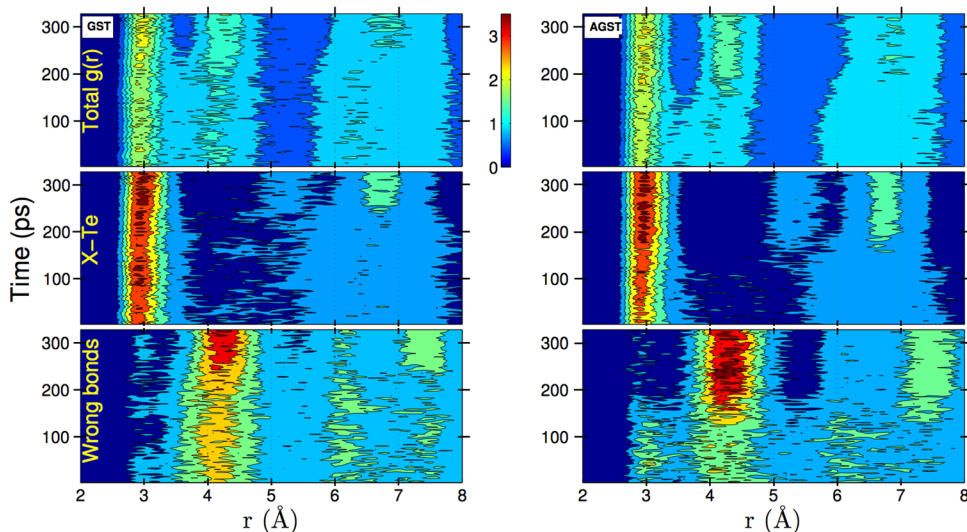


FIG. 3. Evolution of pair correlation functions in  $\text{Ge}_2\text{Sb}_2\text{Te}_5$  (left) and  $\text{Ag}_{0.5}\text{Ge}_2\text{Sb}_2\text{Te}_5$  (right) with time (model 3).

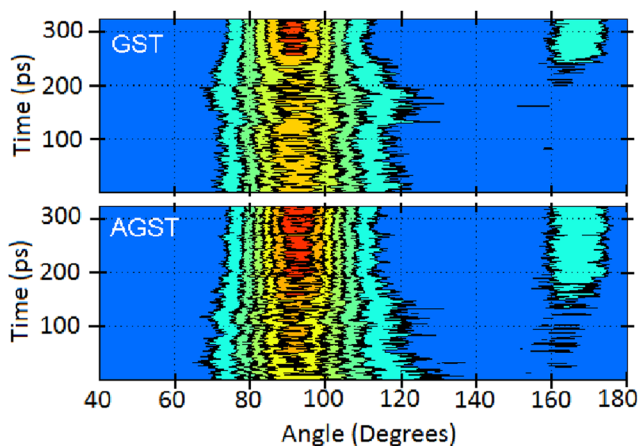


FIG. 4. Time evolution of Ge-centered bond angle distributions in  $\text{Ge}_2\text{Sb}_2\text{Te}_5$  (up) and  $\text{Ag}_{0.5}\text{Ge}_2\text{Sb}_2\text{Te}_5$  (down) (model 3).

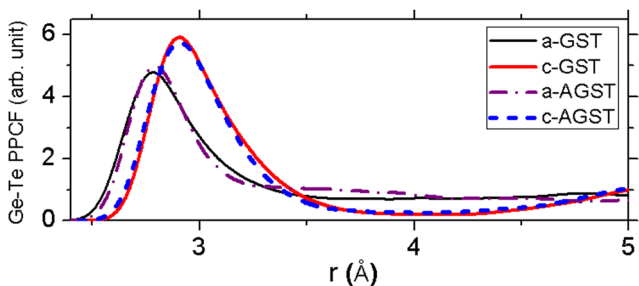


FIG. 5. Ge-Te partial pair correlation functions (PPCFs) at 300 K in both phases of  $\text{Ge}_2\text{Sb}_2\text{Te}_5$  and  $\text{Ag}_{0.5}\text{Ge}_2\text{Sb}_2\text{Te}_5$ .

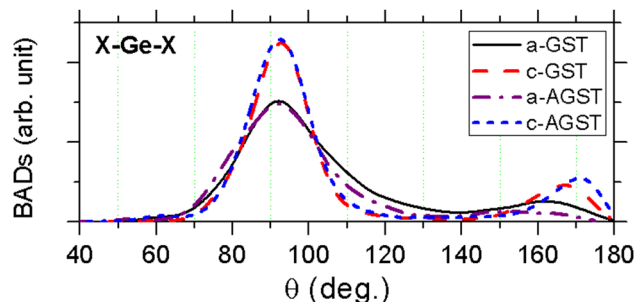


FIG. 6. Ge-centered BADs (model 3) in both phases of  $\text{Ge}_2\text{Sb}_2\text{Te}_5$  and  $\text{Ag}_{0.5}\text{Ge}_2\text{Sb}_2\text{Te}_5$  at 300 K.

GST. This Ag-induced change is also observed in the Ge-centered BAD as a suppression near  $109^\circ$  depicting a reduction in the fraction of tetrahedral Ge sites due to addition of Ag. This reduction caused the increase in the average Ge-Te bond length since Ge-Te bond length with tetrahedral geometry is smaller than Ge-Te with octahedral geometry.<sup>12,13</sup> This reduction in the concentration of tetrahedral Ge sites in AGST can explain the faster crystallization since Ag might have induced the conversion of tetrahedral Ge sites into octahedral Ge sites. In contrast to the amorphous phase, we observed identical Ge-Te bond lengths between GST and AGST in the crystalline phases. This is consistent with the fact that all the tetrahedral Ge changes to an octahedral geometry during crystallization. On the other hand, Ag-induced change is negligible in the Sb-Te PPCF and Sb-centered BAD, in both phases. This is also supported by the fact that Sb always takes octahedral geometry in either of the phases. Beside Ge-Te and Sb-Te bonds pairs, we observed a significant fraction of wrong bonds. These wrong bonds amount to 25% in amorphous phases and fall to about 6% in the crystalline phases. The analysis of the local structure also enables us to identify the interaction of the dopants (Ag atoms) in GST. The Ag PPCF confirms that Ag is mainly bonded to Te rather than to Ge or Sb. This is also true in crystalline phase where Ag takes the vacancy sites (or similar sites as Ge/Sb).

Beside faster crystallization, addition of Ag in GST showed improvement of the material properties. The computation of the atomic densities demonstrates a relatively small density change (4.61%) between the two phases of AGST in contrast to a density change of 6.84% in pure GST. This smaller volume (density) change in Ag-doped GST could result in reduced residual stress in phase change memory (PCM) devices. We further computed the difference in the energies between the amorphous and the crystalline phases in GST and AGST. The energy difference of 80 meV/atom in AGST is about 20 meV/atom more than that of pure GST. This larger energy difference might yield better thermal stability in Ag-doped GST and could improve the data retention capability of PCM devices.

The investigation of the electrical properties [via electronic density of states(EDOS)] in both phases of GST and AGST confirms no major differences in the EDOS, with

TABLE I. Comparison of dielectric constant between the two phases of  $\text{Ge}_2\text{Sb}_2\text{Te}_5$  and  $\text{Ag}_{0.5}\text{Ge}_2\text{Sb}_2\text{Te}_5$  (model 3).

Material	Amorphous	Crystalline	% increase
$\text{Ge}_2\text{Sb}_2\text{Te}_5$	25.9	53.0	105
$\text{Ge}_2\text{Sb}_2\text{Te}_5$ (Ref. 15)	16.0	33.3	108
$\text{Ag}_{0.5}\text{Ge}_2\text{Sb}_2\text{Te}_5$	26.9	60.2	124

p-like states of Te, Sb, and Ge dominating both the valence and the conduction band and Ag contributing a d-like state about 4 eV below the Fermi level. The band gap is observed to decrease with the presence of Ag. Since the larger band gap in a-GST as compared to c-GST is due to the presence of  $\text{sp}^3$ -bonded Ge atoms,<sup>14</sup> the reduced band gap by doping can also be attributed to the reduction of the tetrahedral Ge atoms.

The utility of the PCMs stems from the contrast in optical properties between amorphous and crystalline phases. The imaginary and real parts of the dielectric function confirm that the optical contrast is preserved in AGST. These results are consistent with Shportko *et al.*<sup>15</sup> The estimation of the optical dielectric constant, i.e., the lower energy-limit of the real part of the dielectric function ( $\omega \rightarrow 0$ ) is presented in Table I. We observed a slightly higher dielectric constant in AGST as compared to GST and suspect that this is due to improved medium-range order (increase in the number of four-membered, near-square, rings<sup>1</sup>) in AGST.

In conclusion, we have used AIMD simulations to study the effect of Ag doping in  $\text{Ge}_2\text{Sb}_2\text{Te}_5$ . We were also able to simulate the ultrafast phase transitions from amorphous to crystalline phase. The incubation and crystallization period were found to depend on the wrong bonds present in the amorphous phase. Moreover, our simulation revealed that the crystallization speed is increased by doping  $\text{Ge}_2\text{Sb}_2\text{Te}_5$  with Ag and attribute this faster crystallization of AGST to the reduction of tetrahedral Ge sites due to addition of Ag in GST. Furthermore,

the medium range order is found to be enhanced with the addition of Ag, with an increased number of four membered rings and decreased fraction of tetrahedral Ge. In addition, the larger energy/atom difference between amorphous and crystalline phases also suggests that  $\text{Ag}_{0.5}\text{Ge}_2\text{Sb}_2\text{Te}_5$  is thermally more stable than  $\text{Ge}_2\text{Sb}_2\text{Te}_5$ . On the other hand, smaller density difference in  $\text{Ag}_{0.5}\text{Ge}_2\text{Sb}_2\text{Te}_5$  between the two phases as compared to  $\text{Ge}_2\text{Sb}_2\text{Te}_5$  could well reduce the residual stress in the PCM devices. Finally, the increased optical contrast between the two phases as well as a potential increase in crystallization speed might lead to PCM devices with improved performance.

We thank Professor S. R. Elliott for many helpful conversations. This work was supported by NSF DMR 09-03225 and NSF DMR 09-06825. This work was also supported in part by an allocation of computing time from the Ohio Supercomputer Center.

- <sup>1</sup>J. Hegedüs and S. R. Elliott, *Nature Mater.* **7**, 399 (2008).
- <sup>2</sup>G. Kresse and J. Furthmüller, *Comput. Mat. Sci.* **6**(1), 15–50 (1996).
- <sup>3</sup>G. Kresse and J. Furthmüller, *Phys. Rev. B* **54**(16), 11169–11186 (1996).
- <sup>4</sup>G. Kresse and J. Hafner, *Phys. Rev. B* **47**(1), 558–561 (1993).
- <sup>5</sup>P. E. Blöchl, *Phys. Rev. B* **50**, 17953 (1994).
- <sup>6</sup>G. Kresse and J. Joubert, *Phys. Rev. B* **59**, 1758 (1999).
- <sup>7</sup>J. P. Perdew, K. Burke, and M. Ernzerhof, *Phys. Rev. Lett.* **77**, 3865–3868 (1996).
- <sup>8</sup>D. A. Drabold, *Eur. Phys. J. B* **68**, 1–21 (2009).
- <sup>9</sup>B. Cai, D. A. Drabold, and S. R. Elliott, *Appl. Phys. Lett.* **97**, 191908 (2010).
- <sup>10</sup>T. H. Lee and S. R. Elliott, *Phys. Rev. Lett.* **107**, 145702 (2011).
- <sup>11</sup>A. V. Kolobov, P. Fons, A. I. Frenkel, A. L. Ankudinov, J. Tominaga, and T. Uruga, *Nature* **3**, 703 (2004).
- <sup>12</sup>J.-Y. Raty, C. Otjacques, J.-P. Gaspard, and C. Bichara, *Solid State Sci.* **12**, 193–198 (2010).
- <sup>13</sup>S. Caravati, M. Bernasconi, T. D. Kühne, M. Krack, and M. Parrinello, *J. Phys. Condens. Matter* **21**, 255501 (2009).
- <sup>14</sup>J. Akola and R. O. Jones, *Phys. Rev. B* **76**, 235201 (2007).
- <sup>15</sup>K. Shportko, S. Kremers, M. Woda, D. Lencer, J. Robertson, and M. Wuttig, *Nature Mater.* **7**, 653 (2008).